



Design of a Highly Active Peptide Inhibitor of Farnesyltransferase and Its Protective Effect Against Acute Liver Failure

Chun-Lian Huang¹, Hang-Shuai Qu², A-Li Li¹, Chen-Qian Ying¹, Hui Shao¹, Yong-Zhi Tang¹, Hua-Zhong Chen¹, Tao-Hsin Tung³, Jian-Sheng Zhu¹

¹Department of Infectious Diseases, Taizhou Hospital of Zhejiang Province Affiliated to Wenzhou Medical University, Linhai, Zhejiang, 317000, People's Republic of China; ²Department of Public Laboratory, Taizhou Hospital of Zhejiang Province Affiliated to Wenzhou Medical University, Linhai, Zhejiang, 317000, People's Republic of China; ³Evidence-Based Medicine Center, Taizhou Hospital of Zhejiang Province Affiliated to Wenzhou Medical University, Linhai, Zhejiang, 317000, People's Republic of China

Correspondence: Jian-Sheng Zhu, Department of Infectious Diseases, Taizhou Hospital of Zhejiang Province Affiliated to Wenzhou Medical University, 150 Ximen Street, Linhai, Zhejiang Province, 317000, People's Republic of China, Email zhujs@enzemed.com

Purpose: Acute liver failure (ALF) is a fatal syndrome associated with massive hepatocyte death. Previous studies have found that Farnesyltransferase (FTase) inhibitors improve disease progression in mouse models of endotoxemia, sepsis, and autoimmune hepatitis. PANoptosis is a novel type of programmed cell death (PCD), including pyroptosis, apoptosis, and necrosis, that plays an important role in ALF. This study was designed and investigated whether the FTase inhibitor PD083176 (d2,d3,d5) could attenuate ALF progression by modulating PANoptosis.

Methods: Combining the technical tools of computational biology, structural biology and pharmacology, we designed and obtained three high-affinity human FTase inhibitors of PD083176(d2,d3,d5). Then, these FTase inhibitors were investigated by animal experiments by administering PD083176(d2,d3,d5) (10 mg/kg) before modeling with LPS (100 µg/kg)/D-GaIN (300 mg/kg) or TAA (800 mg/kg).

Results: We found that ALF induced by LPS/D-GaIN or TAA were associated with increased farnesylated protein in the liver. PD083176(d2,d3,d5) not only inhibited hepatic farnesylated proteins but also significantly attenuated liver injury and mortality in ALF mice. Importantly, PD083176(d2,d3,d5) treatment effectively inhibited hepatocyte apoptosis (Bax, Bcl-xL and TUNEL cell counts), pyroptosis (Caspase-1 and GSDMD), and necrotic apoptosis (RIPK1 and RIPK3).

Conclusion: Collectively, these findings demonstrate that PD083176(d2,d3,d5) could alleviate LPS/D-GaIN or TAA-induced ALF by regulating apoptosis, pyroptosis, and necrotizing apoptosis, which might provide a new therapeutic strategy and scalability challenge for ALF.

Keywords: acute liver failure, FTase, PD083176(d2,d3,d5), peptide inhibitor, PANoptosis

Introduction

Acute liver failure (ALF) is a lethal syndrome characterized by sudden death of a large number of hepatocytes and rapid deterioration of liver function. ALF worldwide is estimated to affect approximately 1 to 6 individuals per million annually.^{1–3} There are many etiologies that contribute to ALF, including acetaminophen, viruses, malignancies, and autoimmune and rare genetic/metabolic disorders.⁴ The most effective treatment for patients with acute failure is liver transplantation.⁵ Even after successful liver transplantation, the disease mortality rate can still reach up to 30%.⁶ However, factors such as liver source and cost have severely limited the widespread use of liver transplantation.⁷ Therefore, there is a need to develop new preventive and/or therapeutic strategies to improve clinical outcomes in patients with ALF.

The pathophysiologic mechanism of ALF is a complex process involving a complex interplay of hepatocyte death, inflammatory and immune responses, hemodynamic alterations and metabolic disturbances.^{8,9} In 2020, Christian et al proposed and revealed the concept of PANoptosis.¹⁰ PANoptosis, a unique new form of programmed cell death (PCD), is characterized by pyroptosis, apoptosis, and necrosis. PANoptosis can lead to the release of a variety of inflammatory cytokines and cytokine storms, and is implicated in the pathogenesis of a wide range of diseases.^{11,12} Li, Wenyuan et al found that increased TAK1 expression reduced the extent of cell damage and PANoptosis in an ALF model.¹³ Shi, Chunxia et al found that the LPS/D-GalN group had elevated levels of the PANoptosis-related molecules RIPK1, GSDMD, caspase-3, MLKL, IL-18, and IL-1.¹⁴ Thus, many studies found that PANoptosis plays an important role in ALF.

Farnesyltransferase (FTase) is a substrate for more than 100 proteins, which are involved in several physiological processes such as signal transduction, vesicular transport, and cell cycle.¹⁵ Studies have shown that FTase is strongly associated with several diseases such as tumors, neurodegenerative diseases, retinitis pigmentosa, and liver diseases.^{16–19} PD083176, a peptide inhibitor of FTase, was earlier used as a potential candidate for antitumor drug.²⁰ However, the poor permeability makes it difficult to reach effective concentration in vivo. To address the poor tissue permeability of PD083176, we constructed a binding model of FTase and PD083176, structurally optimized PD083176 based on the above model and designed a suitable dosage form to improve the water solubility and membrane permeability of PD083176 thus obtaining a potentially highly active FTase peptide inhibitor PD083176(d2,d3,d5).

In this study, we investigated the therapeutic effect of PD083176(d2,d3,d5) by two models of ALF (LPS/D-GalN and TAA). We found that PD083176(d2,d3,d5) not only inhibited the inflammatory response, but also inhibited PANoptosis. Importantly, peptide drugs have the advantages of low toxicity and high efficiency compared with small molecule drugs. We designed and developed a highly active peptide drug targeting FTase will have the potential to enter the clinic, which is expected to broaden the drug therapy strategy for ALF and provide a new direction for the treatment of ALF.

Materials and Methods

Construction of FTase Peptide Inhibitors

Design of FTase Peptide Inhibitors

In our previous studies, we used Molecular Dynamics simulations (MD) to carry out kinetic studies on a series of target FTase/peptide complex systems.²¹ PD083176 is a competitive inhibitor of FTase peptide substrates reported in the 1990s. We first constructed structural models of the human- and murine-derived FTase-peptide complexes with PD083176 complex structural model. The interaction forces (such as hydrogen bonding, van der Waals force, electrostatic attraction, desolvation effect and entropy penalty) between PD083176 and FTase were comparatively analyzed, and the contribution of each amino acid residue in the sequence of PD083176 to the interaction was calculated in BioPython software. Subsequently, we performed systematic substitution of individual residues (motifs) of PD083176 and calculated the effect on activity. Favorable substitutions at each residue (motif) positions were combined to obtain 12 ($4 \times 3 \times 1$) PD083176 derivatives.

High Performance Liquid Chromatographic Preparation of FTase

A small amount of sample was taken in a 0.5 mL centrifuge tube and dissolved by sonication with Acetonitrile (ACN) +H₂O until clarified and filtered into the sample. Analyze with gradient 10–100%. Weigh 330 mg of sample in a 100 mL beaker, add 10mL (ACN+H₂O) and dissolve it by ultrasonication, after the sample is completely dissolved, filter it through 0.45 μ m filter membrane. The High Performance Liquid Chromatography (HPLC) was equilibrated with preparative conditions (220 nm wavelength, 30 mL/min flow rate, 30 mm*250 mm C18 preparative column) for about 10 min, then the sample was injected through the inlet valve, a preparative gradient was run (0 min 37 gradient) and fractions were collected in segments, and the pump was stopped at the end of the gradient run. The collected fractions were taken and analyzed sequentially with a gradient of 35–60% to 95% purity, which is considered a qualified sample. Qualified samples will be rotary evaporator will be the solution of organic solvents spin evaporated off after freeze-

drying on the freeze dryer freeze-drying. After two days of freeze-drying, the sample was taken out and weighed into EP tubes for storage.

Basic Experiments

Reagents

The FTase peptide inhibitors PD083176(d2,d3,d5) was designed in-house, and synthesized by Gill Biochemicals (Shanghai) Co. LPS, D-GaIN, and TAA were purchased from Sigma-Aldrich (St. Louis, MO). FTase (Cat# GTX85881) was purchased from Gene Tex (Calif, USA). Bcl-2 (Cat# CY5032), Bcl-xl (Cat# CY5452), Caspase-3 (Cat# CY5384), β -actin (Cat# AY0573), NF- κ B (Cat# AB3449), Caspase-1 (Cat# DY1200) were purchased from Abways (Shanghai, China). GSDMD (Cat# ab209845), ASC (Cat# ab32499), IL-1 β (Cat# ab283818), Caspase-1 (Cat# ab179515), ASC (Cat# ab309497), MLKL (Cat# ab196436), RIPK1 (Cat# ab300617), RIPK3 (Cat# ab255705) were purchased from Abcam (USA). NLRP3 (Cat# 15101) was purchased from cell signalling technology (CST, USA). Dimethyl sulfoxide (DMSO) was purchased from MCE (Shanghai, China, Cat# HY-Y0320). Total RNA was reverse transcribed to cDNA with a PrimeScript RT Reagent Kit (Takara, RR036A). TB Green Premix Ex Taq (Takara, R420A) was used for real-time quantitative PCR. Microtiter plate assay kits for glutamic oxalacetic transaminase (AST, Cat# C00-2-1) and glutamic-pyruvic transaminase (ALT, Cat# C009-2-1) were purchased from Nanjing Jianjian Bioengineering Institute (Nanjing, China). Enzyme-linked immunosorbent assay (ELISA) kits for serum tumor necrosis- α (TNF- α , Cat# E-MSEL-M0002), interleukin-1 β (IL-1 β , Cat# E-MSEL-M0003) and interleukin-6 (IL-6, Cat# E-MSEL-M0001) were purchased from Elabscience (Wuhan, China).

Animal and Drug Treatment

Male C57BL/6J mice (7–8 weeks old; weighing 23–25 g) were provided by Shanghai Slaughter Laboratory Animal Technology Company (Shanghai, China). Animal experiments were approved by the Animal Experimentation Ethics Committee of Taizhou Hospital, Zhejiang Province (Approval No. tzy-2022154). The 3Rs guidelines for animal welfare were followed for in vivo studies. Mice were placed in standard cages under light-controlled conditions (12 h light-dark cycle), maintained at 25°C, and fed and watered ad libitum. In the present study, following two ALF mouse models were constructed.

- (1) The first one: mice were intraperitoneally injected with D-GaIN and LPS, and this modeling method has been widely used in animal models of ALF.^{22,23} Thirty mice were randomly divided into five groups (n=6): control group, LPS/D-GaIN group, and LPS/D-GaIN + PD083176(d2,d3,d5) group.
 - (i) Control group: the same volume of PBS was injected during the experiment;
 - (ii) LPS/D-GaIN group: mice were injected intraperitoneally with LPS (100ug/kg) and D-GaIN (300mg/kg). LPS and D-GaIN could be completely dissolved in PBS.
 - (iii) LPS/D-GaIN+ PD083176(d2,d3,d5) group: the dose of 10 mg/kg of the three inhibitors was selected with reference to previously published literatures.^{21,22} Inhibitors were solubilized with DMSO (2.5 mg/mL). 10 mg/kg inhibitor was injected intraperitoneally into mice 1 h before LPS/D-GaIN treatment.

Mice were euthanized with 1% pentobarbital 6 h after LPS/D-GaIN administration, and blood and liver tissue samples were collected.

- (2) The Second one: as a common hepatotoxin, TAA is also commonly used in animal models of ALF.^{24,25} Thirty mice were randomly divided into 5 groups (n=6): control group, TAA group and TAA+PD083176(d2,d3,d5) group. The mouse ALF model was established by intraperitoneal injection of TAA (800 mg/kg). TAA could be completely dissolved in PBS solution. Mice in the TAA+PD083176(d2,d3,d5) group were injected intraperitoneally with 10 mg/kg PD083176(d2,d3,d5) one hour prior to the TAA treatment. 24 h after TAA administration mice were euthanized with 1% pentobarbital and blood and liver tissue samples were collected.

Survival Experiment

To investigate the effects of PD083176(d2,d3,d5) on the survival of LPS/D-GaIN-induced ALF mice, the mice were divided into the control group, LPS/D-GaIN group and LPS/D-GaIN+PD083176(d2,d3,d5) group (n=10). After the intervention injection of LPS/D-GaIN and PD083176(d2,d3,d5), the mortality rate of animals in each group was observed every 2 h and the number of survived animals was recorded for 12 h.

Serum Biochemical Assay

Blood was collected in non-anticoagulated tubes and serum was separated by centrifugation at 4000 rpm for 10 min at 4°C. Serum ALT and AST were measured using biochemical assay kits to assess liver injury. Serum IL-1 β , TNF- α , and IL-6 levels were determined using enzyme-linked immunosorbent assay (ELISA) kits according to the manufacturer's protocol.

Histopathologic Staining (H&E Staining)

Fresh liver tissues were fixed in 4% neutral buffered formalin for 24 h. Liver specimens were sectioned to 5 μ m thickness. Sections were stained with hematoxylin and eosin according to standard histologic methods. Liver pathologic changes were observed and evaluated under light microscopy. Liver histology scoring was used to determine the degree of liver injury, which was divided into inflammation scoring and necrosis scoring.^{26,27} In the scoring system, no inflammatory response was recorded as 0, mild inflammatory response (< 10% of liver sections) as 1, moderate inflammatory response (10–50% of liver sections) as 2, and severe inflammatory response (> 50% of liver sections) as 3. Absence of necrosis was recorded as 0, necrotic area < 10% was recorded as 1, necrotic area 10–25% was recorded as 2, and necrotic area > 25% was recorded as 3.

TUNEL (TdT-Mediated dUTP Nick End Labeling)

TUNEL staining used to measure the cell death in liver tissues. According to the manufacturer's instructions (Roche, United States). Liver sections were incubated with proteinase K for 15 min at 37°C and then washed with phosphate buffered saline (PBS). Sections were incubated with TUNEL reaction mixture at 37°C for 1 h. Cell nuclei were stained with DAPI (Propidium iodide) for 5 min (Beyotime, China). TUNEL-positive cells were observed and analyzed by fluorescence microscopy.

Immunohistochemistry (IHC)

Paraffin-embedded liver tissues were sectioned and then subjected to the following operations: degumming, rehydration and antigen recovery by boiling the sections in sodium citrate buffer (10 mm sodium citrate, 0.05% Tween 20, pH 6.0) and blocked at room temperature (RT) (1% BSA, 1 h). Sections were then incubated with primary antibodies FTase (1:500) placed at 4°C overnight and then incubated with the appropriate secondary antibody. The prepared DAB chromogenic solution working solution was added dropwise to the tissue sections, and the color was developed for 10 min and observed under the microscope. The stained area was calculated using Image J software (BioRad, USA).

Real-Time Quantitative Total RNA (RT PCR) Extraction From Cultured Cells by Trizol Method

PrimeScrip™ RT kit from Takara (Japan) and polymerase chain reaction equipment from Bio-Rad (USA) were used. The cDNA was amplified using an ABI7500 real-time PCR instrument (Applied, USA) and TB Green®PreMix Ex Taq™II (Takara, Japan). The cycling threshold (Ct) was calculated and normalized to the level of housekeeping gene (18s). The expression of each group of target genes was detected by the 2- $\Delta\Delta$ Ct method. As shown in Table 1.

Western Blot Analysis

Ground tissues were lysed with radioimmunoprecipitation assay buffer (RIPA, Beyotime Biotechnology, P0013B), Phenylmethanesulfonyl fluoride (PMSF, Beyotime Biotechnology, ST505) and phosphatase inhibitors on ice and

Table 1 Primer Sequence

Species	Primer name (Forward/Reverse)	Primer Sequence (5'-3')
Mus	IL-1 β -F	AGTTGACGGACCCCAAAAG
Mus	IL-1 β -R	AGCTGGATGCTCTCATCAGG
Mus	IL-6-F	GCTGGTGACAACCACGGCCT
Mus	IL-6-R	CTGCAAGTGCATCATCGTTGT
Mus	TNF- α -F	AGCCACGTCGTAGCAAACC
Mus	TNF- α -R	GGAAGCGTGGTGGTTTGCTA
Mus	I8s-F	ACTCAACACGGGAAACCT
Mus	I8s-R	CGCTCCACCAACTAAGAA

centrifuged at 12,000 rpm, 4°C for 15 min. Protein concentration was determined using the BCA Protein Analysis Kit (Beyoncé, Shanghai) according to the manufacturer's instructions. 40 μ g of protein was separated by 8–12% SDS-PAGE and blotted on PVDF membrane (Millipore, CA, USA). After being blocked with skimmed milk for 2 h, the membranes were incubated at 4°C overnight with antibodies of Bcl-2 (1: 1000), Bcl-xl (1: 1000), Caspase-3 (1: 1000), Bax (1: 1000), pro-Caspase-3 (1: 1000), NLRP3 (1: 1000), ASC (1: 1000), IL-1 β (1: 1000), Caspase-1 (1: 1000), NF- κ B (1: 5000), RIPK1 (1: 1000), RIPK3 (1: 1000), MLKL (1: 1000) and β -actin (1: 1000). Then washed and incubated with corresponding secondary antibodies at room temperature for 1 h. Membranes were washed 3 times using TBST for 5 min each time, incubated in the appropriate HRP-conjugated secondary antibody for 1 h at room temperature with shaking, and then again washed 3 times with TBST for 5 min each time. After cutting the membrane horizontally according to the position of the target protein, protein-antibody complexes were detected on an ImageQuant LAS-500 imaging system (GE Health Care, USA) using enhanced chemiluminescence reagents (Millipore, USA). Finally, ImageJ software (NIH, USA) was used to quantify and analyze the bands were quantified and analyzed.

Double Immunofluorescence

For immunofluorescence staining, frozen liver tissue sections were fixed with Perfluoroalkoxy alkane (PFA), permeabilized with 0.3% Triton X-100 for 20 min, and then blocked with 5% bovine serum albumin for 1 h. Afterwards, slides were incubated with primary antibodies against FTase, NLRP3 at 4°C overnight and then with fluorescent secondary antibodies. DAPI was used for nuclear imaging. Images were taken on a confocal microscope (Nikon A1).

Statistical Analysis

All data were expressed as mean \pm standard deviation (SEM). Data were analyzed by ANOVA using the Prism 9 software package (GraphPad software, La Jolla, CA). Difference was compared using one-way ANOVA followed by Tukey post hoc tests. Kaplan-Meier survival analysis was performed using Log rank test. P values less than 0.05 were considered significant.

Results

Design and Optimization of FTase Inhibitor Using Structural Bioinformatics

In our previous studies, we used MD to carry out kinetic studies on a series of target FTase/peptide complex systems. PD083176 is a competitive inhibitor of FTase peptide substrates reported in the 1990s. We first constructed human and murine FTase and PD083176 complex structural model (Figure 1A and B). Through this model, the interaction forces (such as hydrogen bonding, van der Waals force, electrostatic attraction, desolvation effect and entropy penalty) between

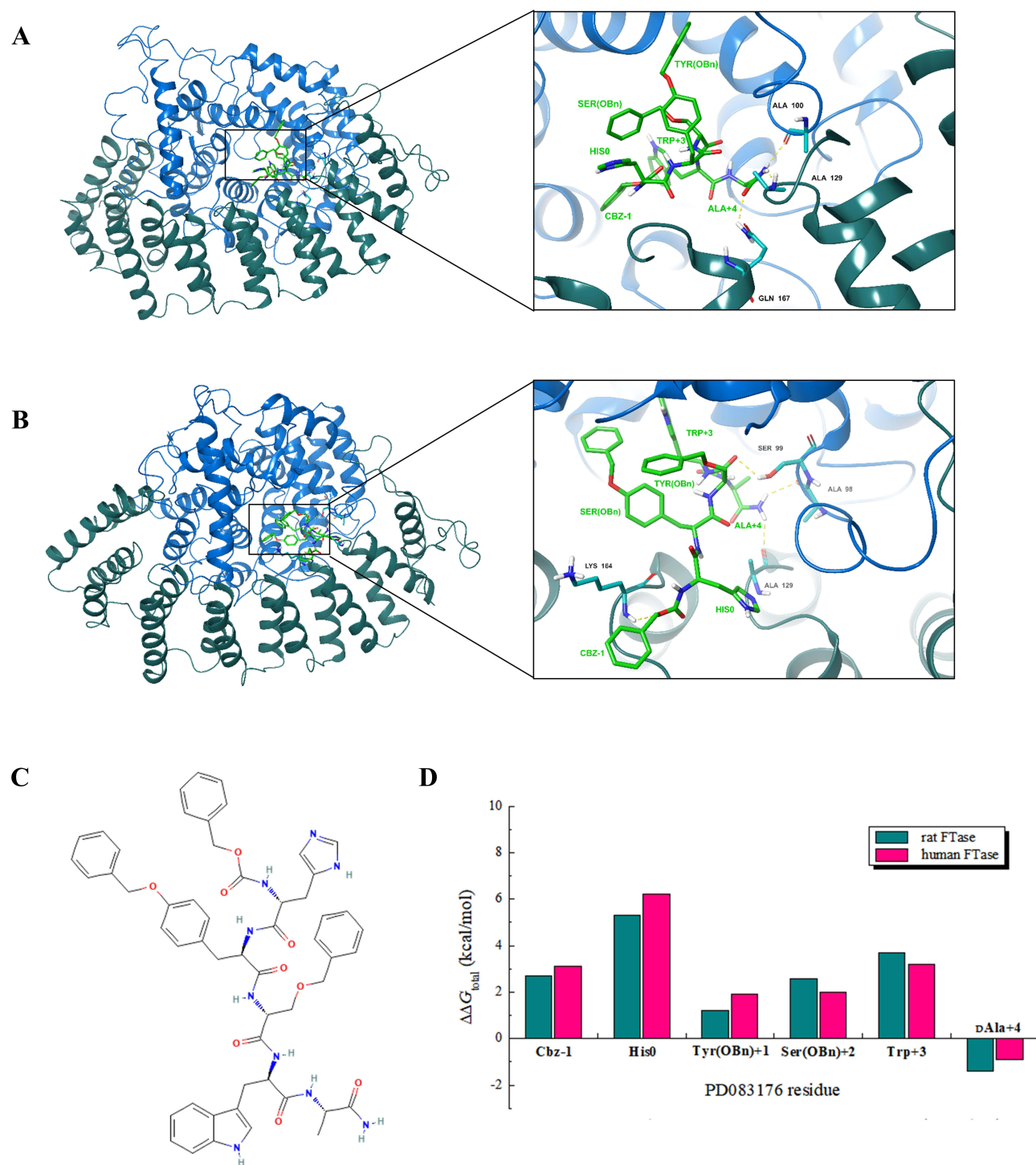


Figure 1 Design optimization of the FTase peptide inhibitor PD083176(d2,d3,d5) using structural bioinformatics. **(A)** Structure of the murine-derived FTase/PD083176(d2, d3,d5) complex (containing FPT-II and Zn^{2+}) constructed by molecular simulation as well as details of its active site; **(B)** Structure of human-derived FTase/PD083176(d2,d3, d5) complex (containing FPP and Zn^{2+}) constructed by molecular mimicry and details of its active site; **(C)** Molecular formula of PD083176. **(D)** Contributions of individual amino acid residues of PD083176(d2,d3,d5) to the affinity of human and murine FTase as calculated using the alanine scanning technique. $\Delta\Delta G_{\text{total}} > 0$ represents a favorable contribution and $\Delta\Delta G_{\text{total}} < 0$ represents an unfavorable contribution.

Table 2 Free Energy ΔG_{total} (Affinity) of PD083176 and Its 12 Derivatives for FTase Binding of Human Origin

Inhibitor	Sequence ^a	ΔG_{total} (kcal/mol)
PD083176	Cbz-His-Tyr(OBn)-Ser(OBn)-Trp-DAla-NH ₂	-29.4
PD083176-d1	Cbz-His- Phe-Thr(OBn) -Trp- Ala -NH ₂	-32.6
PD083176-d2	Cbz-His- Phe-Cys -Trp- Ala -NH ₂	-38.0
PD083176-d3	Cbz-His- Phe-Cys(SBn) -Trp- Ala -NH ₂	-36.4
PD083176-d4	Cbz-His- HomoPhe-Thr(OBn) -Trp- Ala -NH ₂	-31.9
PD083176-d5	Cbz-His- HomoPhe-Cys -Trp- Ala -NH ₂	-36.7
PD083176-d6	Cbz-His- HomoPhe-Cys(SBn) -Trp- Ala -NH ₂	-33.8
PD083176-d7	Cbz-His- Glu-Thr(OBn) -Trp- Ala -NH ₂	-28.5
PD083176-d8	Cbz-His- Glu-Cys -Trp- Ala -NH ₂	-35.6
PD083176-d9	Cbz-His- Glu-Cys(SBn) -Trp- Ala -NH ₂	-34.2
PD083176-d10	Cbz-His- Tyr(OPO₃H₂) -Thr(OBn)-Trp- Ala -NH ₂	-33.0
PD083176-d11	Cbz-His- Tyr(OPO₃H₂) -Cys-Trp- Ala -NH ₂	-37.3
PD083176-d12	Cbz-His- Tyr(OPO₃H₂) -Cys(SBn)-Trp- Ala -NH ₂	-36.1

Note: ^aSubstituted residues (groups) are marked in bold font.

PD083176 and FTase were comparatively analyzed, and the contribution of each amino acid residue in the sequence of PD083176 to the interactions was calculated (Figure 1C and D). We modeled the changes in inhibitory activity due to systematic substitution of individual residues (motifs) of PD083176, and finally systematically combined the favorable substitutions at each residue (motif) position to obtain 12 ($4 \times 3 \times 1$) PD083176 derivatives. Binding free energies (affinities) of these 12 designed derivatives for human FTase are calculated and listed in Table 2. The affinity of most of the designed derivatives is significantly improved compared to PD083176.

In addition, we simulated the structural model of the complexes of human FTase with the best-designed peptide derivatives, PD083176(d2, d3, d5) and analyzed the bonding of the human FTase with PD083176(d2, d3, d5) and the molecular formula of the human FTase in this model (Figure 2A–C).

Effect of PD083176(d2,d3,d5) on Hepatic Farnesylated Proteins in LPS/D-GaIN and TAA-Induced ALF Mice

Immunohistochemical assay showed that farnesylated proteins were increased in the liver 6 h after LPS/D-GaIN stimulation. PD083176(d2, d3, d5) attenuated the elevated farnesylated proteins in the liver. Farnesylated proteins were predominantly expressed in hepatocytes under high magnification, and low expression of control Farnesylated proteins was also present (Figure 3A and B). Similarly, in the TAA-induced ALF mouse model, farnesylated proteins were increased in the liver, and pretreatment with PD083176 (d2, d3, d5) inhibited the expression of farnesylated proteins (Figure 3C and D).

PD083176(d2,d3,d5) Can Have a Protective Effect on LPS/D-GaIN-Induced ALF Mice

Liver morphology showed severe liver injury in LPS/D-GaIN-induced ALF mice. Whereas, there were no significant changes in the control and PD083176 (d2, d3, d5) groups (Figure 4A). In 12 h survival experiment, all mice in the LPS/D-GaIN group were died after 8 h of administration. When treated with PD083176 (d2, d3, d5), the survival rate was approximately 60% in the LPS/D-GaIN+PD083176-d2 group, 50% in the LPS/D-GaIN+PD083176-d3, and 40% in the LPS/D-GaIN+PD083176-d5 group (Figure 4B). H&E showed that that the LPS/D-GaIN group had more severe

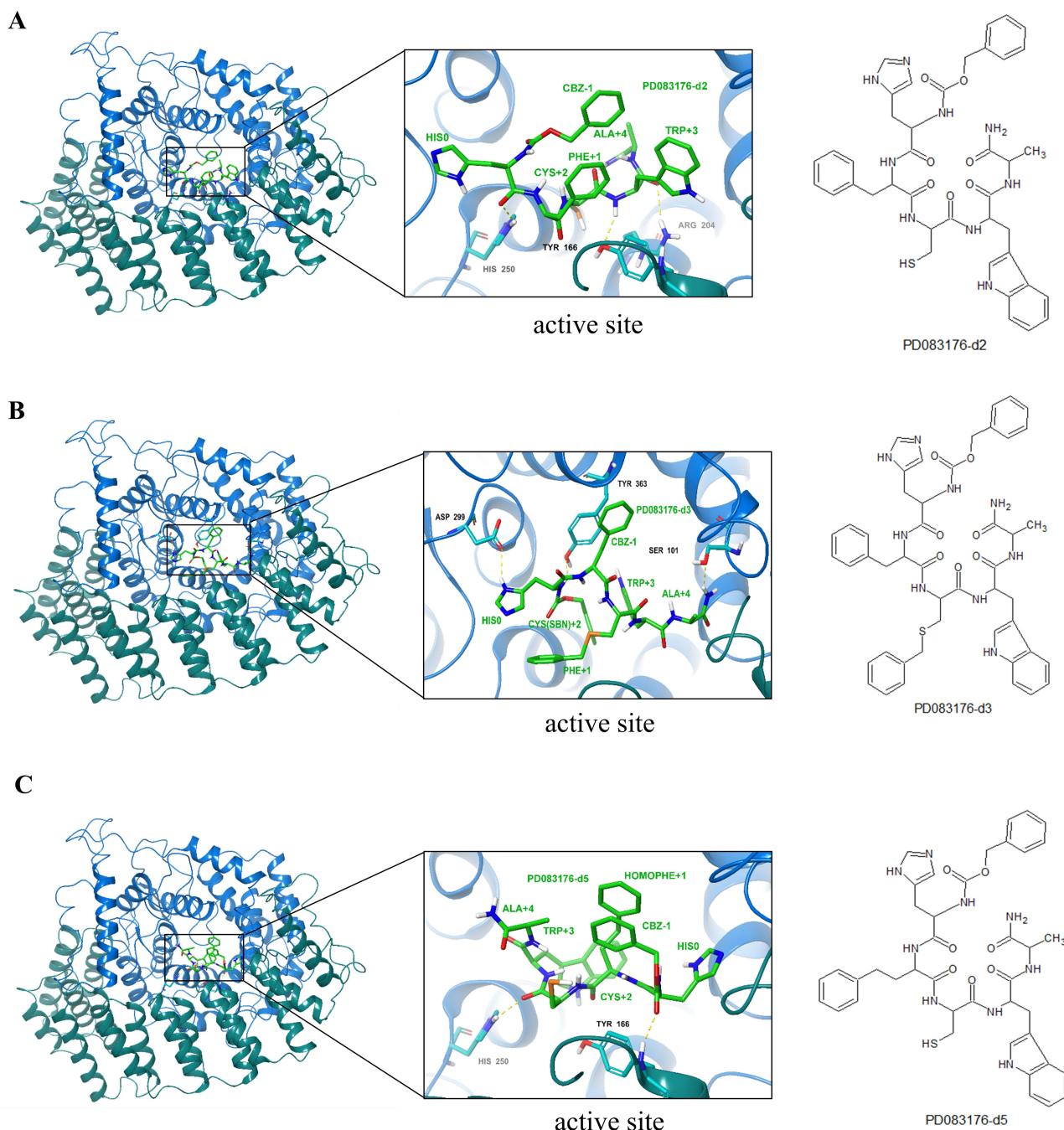


Figure 2 Molecular simulation of docking and molecular formula of FTase peptide inhibitor PD083176(d2, d3, d5). **(A)** Structure of the human FTase/PD083176-d2 complex constructed by molecular simulation along with its active site details and molecular formula; **(B)** Structure of the human FTase/PD083176-d3 complex constructed by molecular mimicry along with its active site details and molecular structural formula; **(C)** Structure of the human FTase/PD083176-d5 complex constructed by molecular modeling along with its active site details and molecular formula.

structural destruction of liver tissue, a larger area of necrosis, and an increased number of infiltrating inflammatory cells compared with the control group. However, the area of liver necrosis and injury was reduced in the PD083176 (d2, d3, d5) group (Figure 4D). Compared with the LPS/D-GaIN group, PD083176 (d2, d3, d5) reduced the liver histologic score (Figure 4C). Serum AST and ALT levels were measured to assess the extent of liver function impairment. Both ALT and AST levels were significantly elevated in model mice, whereas PD083176 (d2, d3, d5) treatment decreased ALF serum ALT and AST levels (Figure 4E and F).

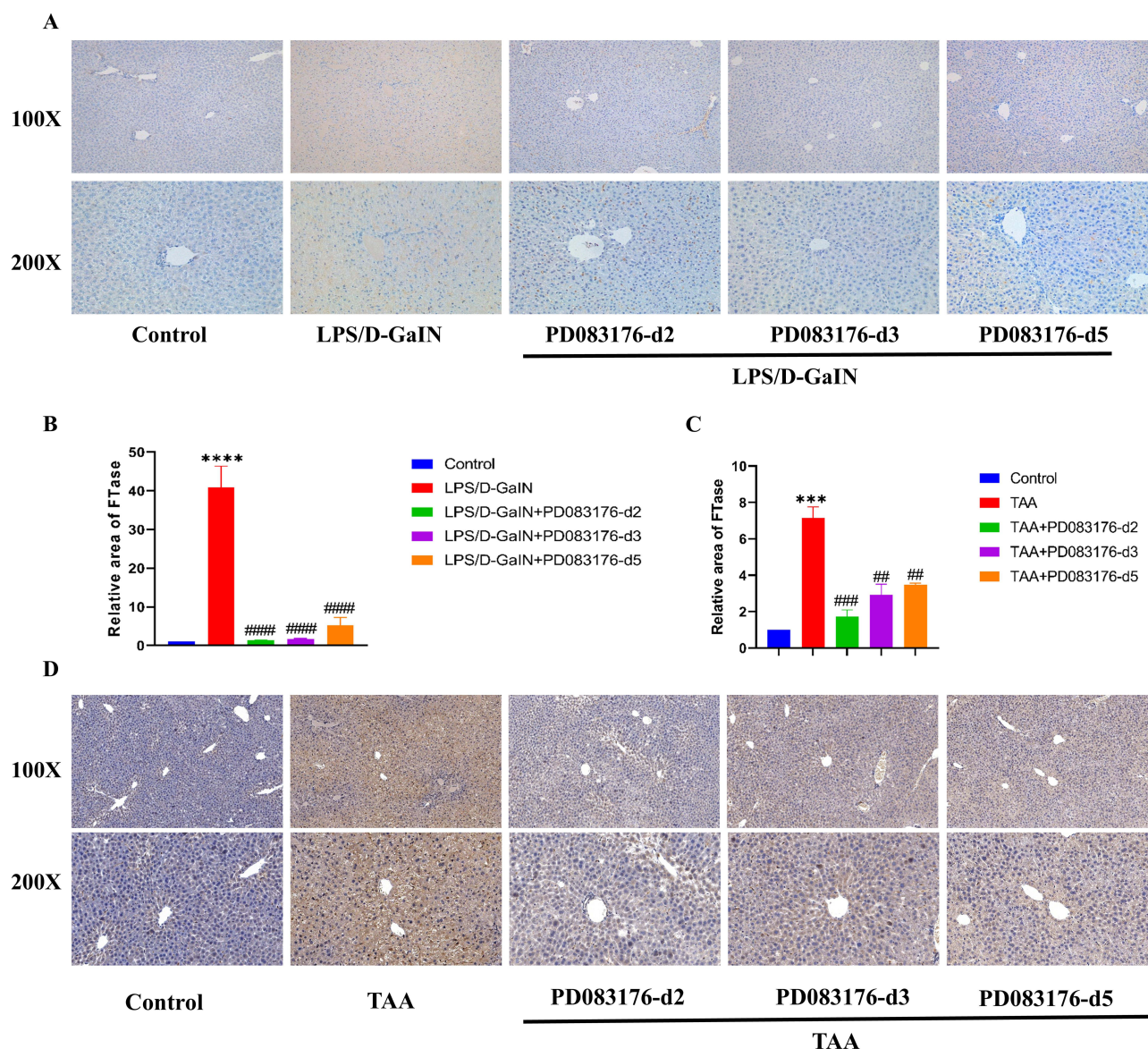


Figure 3 Effect of PD083176(d2,d3,d5) on liver farnesylated proteins in LPS/D-GaIN or TAA-induced ALF mice. **(A)** Immunohistochemical assessment of farnesylated protein expression in LPS/D-GaIN-induced ALF mouse model; **(B and C)** Mean optical density of immunohistochemical staining of FTase in different ALF models. **(D)** Immunohistochemical assessment of farnesylated protein expression in TAA-induced ALF mouse model; Compared with the control group, *** $p < 0.001$, **** $p < 0.0001$. ## $p < 0.01$, #### $p < 0.001$, ##### $p < 0.0001$ compared with the LPS/D-GaIN group. $n = 6$ for each group data are expressed as mean \pm SEM.

PD083176(d2,d3,d5) Is Protective Against TAA-Induced ALF Mice

Liver morphology showed severe liver injury in TAA-induced ALF mice, whereas there were no significant changes in the control and PD083176(d2,d3,d5) groups. HE staining showed more severe structural destruction of the liver tissue, larger necrotic area, and an increased number of infiltrating inflammatory cells in the TAA group compared with the control group. However, the area of liver necrosis and injury was reduced in the PD083176(d2,d3,d5) groups (Figure 5A). Compared with the model group, PD083176(d2,d3,d5) decreased the liver histologic score (Figure 5B). Serum AST and ALT levels assessed the extent of hepatic impairment. Both ALT and AST levels were significantly elevated in model mice, whereas PD083176 (d2, d3, d5) treatment decreased ALF serum ALT and AST levels (Figure 5C and D). ELISA results showed that the serum levels of inflammatory cytokines such as TNF- α , IL-6, and IL-1 β were elevated in the model mice compared to normal mice. Treatment with PD083176 (d2, d3, d5) reduced these cytokine levels (Figure 5E–G).

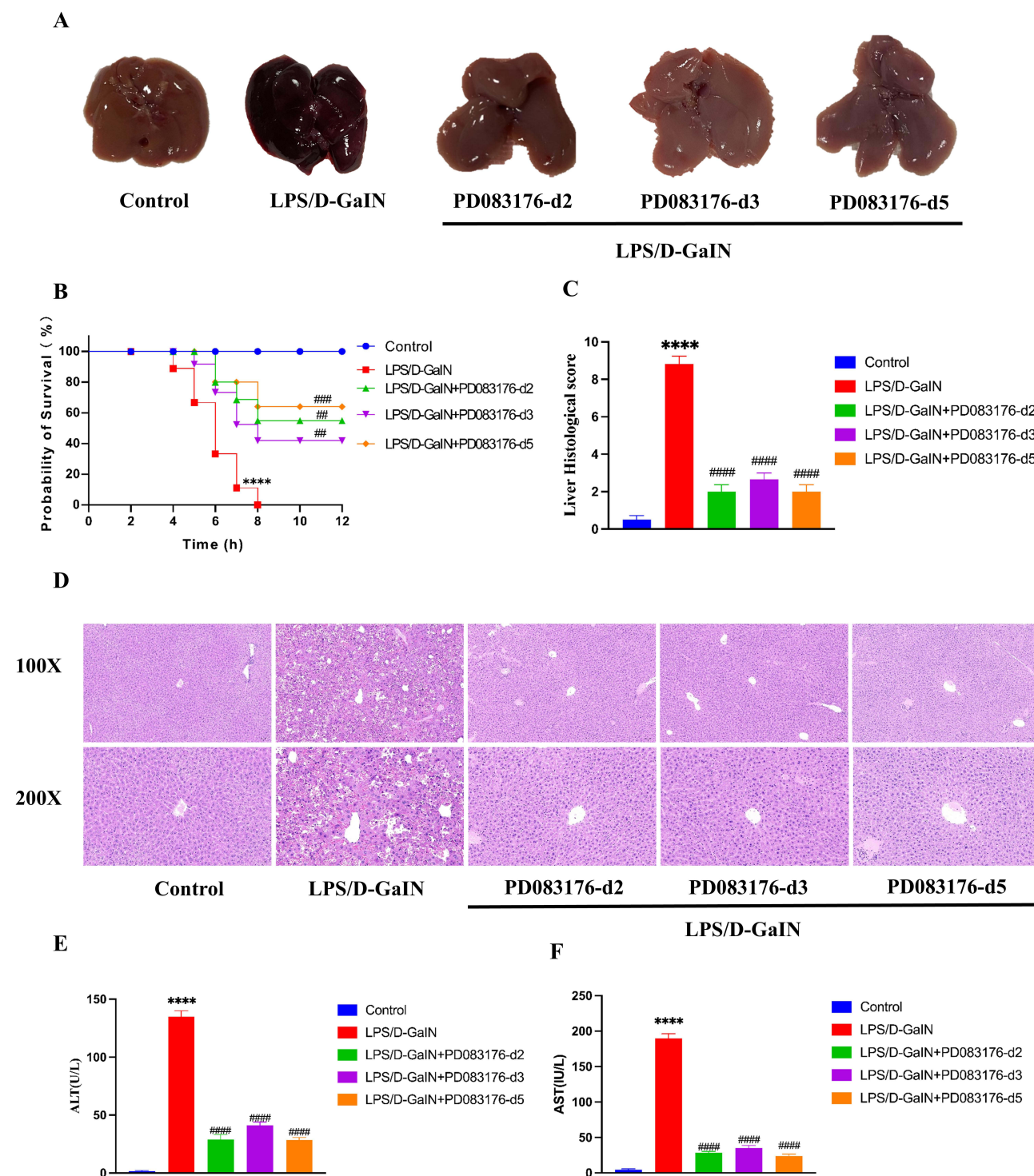


Figure 4 Effect of PD083176(d2,d3,d5) on liver morphology, liver histology scores and survival in ALF mice. **(A)** Liver morphological changes; **(B)** Survival rate at 12 h in each group of mice; **(C)** Histological scores of liver tissues; **(D)** HE-stained liver tissues; serum AST **(E)** and ALT **(F)** levels. Compared with the control group, **** $p < 0.0001$. Compared with the LPS/D-GalN group, ### $p < 0.01$, #### $p < 0.001$, ##### $p < 0.0001$. $n = 6$ for each group data are expressed as mean \pm SEM.

Hepatocyte apoptosis is a key factor in TAA-induced ALF model. TUNEL assay confirmed the protective effect of PD083176(d2,d3,d5) on TAA-induced hepatocyte apoptosis. More apoptotic cells were observed in the TAA group, and PD083176(d2,d3,d5) pretreatment decreased the proportion of apoptotic cells (Figure 5H and I). Liver morphology, liver

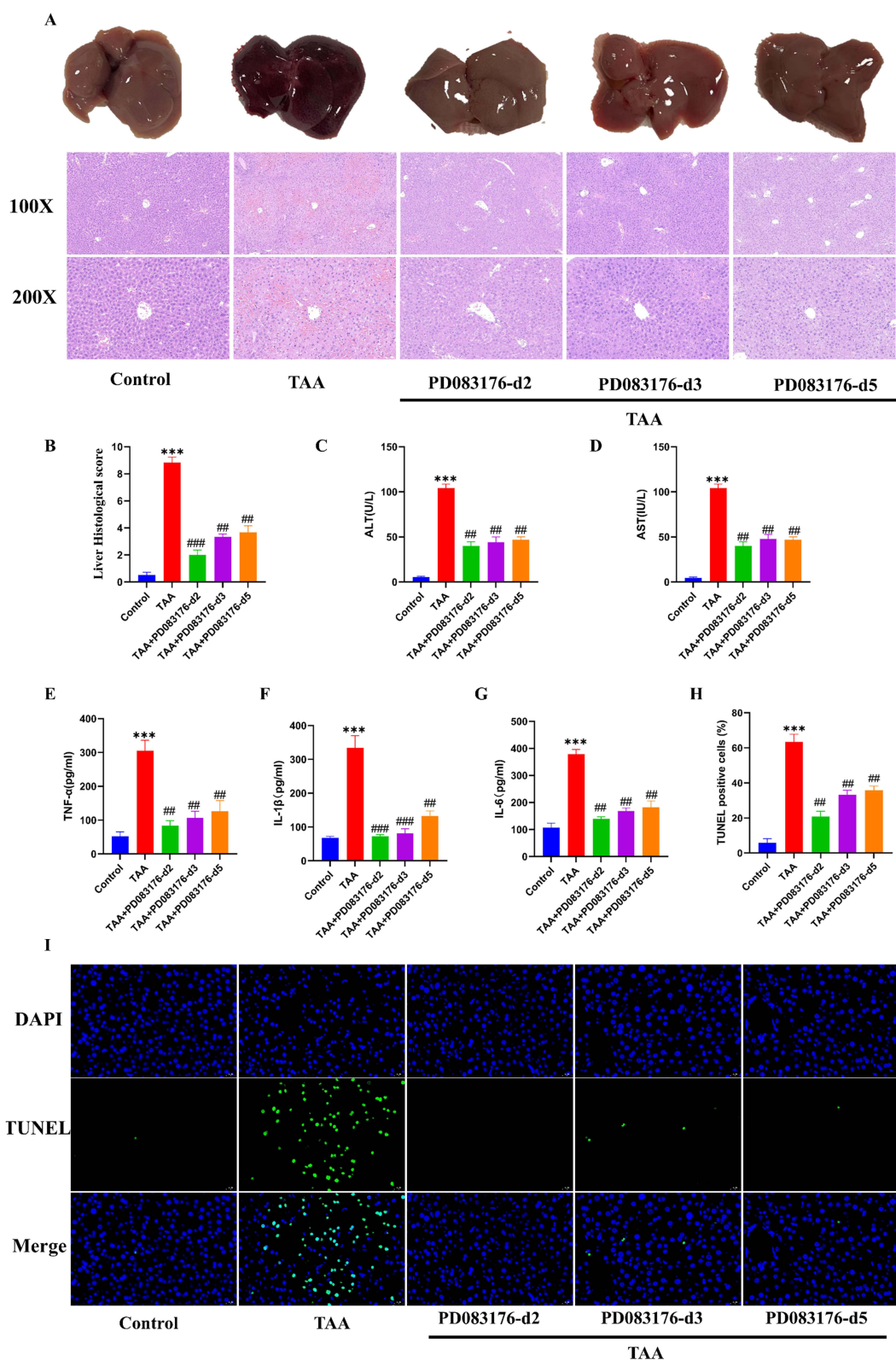


Figure 5 Effects of PD083176(d2,d3,d5) on liver morphology, liver histology score, liver function, and inflammatory response in TAA-induced ALF mice. **(A)** Liver morphological changes and HE staining of liver tissue; **(B)** Liver tissue histologic scores; **(C)** Serum ALT levels; **(D)** Level of serum AST; **(E–G)** Serum levels of TNF- α , IL-1 β and IL-6 expression; **(H)** Quantification of apoptosis; **(I)** Apoptotic cells of liver samples were measured by TUNEL staining. Compared with the control group, *** $p < 0.001$. Compared with the /LPS/D-GalN group, ## $p < 0.01$, ### $p < 0.001$. $n = 6$ for each group data are expressed as mean \pm SEM.

pathological histology, liver function and TUNEL assay confirmed the protective effect of FTase peptide inhibitor PD083176(d2,d3,d5) on TAA-induced ALF mice.

The FTase Inhibitor PD083176(d2,d3,d5) Inhibits the Inflammatory Response and PANoptosis in a Mouse Model of ALF

FTase inhibitor PD083176(d2,d3,d5) suppresses PANoptosis in a mouse ALF model. Hepatocyte apoptosis is a key factor leading to acute liver injury. As shown in Figure 5A, more apoptotic cells were observed in the model group, while PD083176(d2,d3,d5) pretreatment reduced the percentage of apoptotic cells (Figure 6A and B). WB was used to detect the expression of relevant proteins. The results showed that the expression of anti-apoptotic proteins Bcl-2, Bcl-xl, and Caspase-3 was down-regulated, and the expression of pro-apoptotic proteins Bax, and Caspase-3 was up-regulated in the model group. However, PD083176(d2,d3,d5) partially reversed the apoptosis progression (Figure 6C–H). These data indicate reduced apoptosis in the liver of PD083176(d2,d3,d5) ALF mice. These results suggested that PD083176(d2,d3,d5) inhibits apoptosis in ALF liver tissues.

We next found that LPS/D-GaIN induced activation of the NF- κ B pathway and activation of NLRP3 inflammatory vesicles, leading to the onset of pyroptosis in the liver tissue of ALF mice. Immunofluorescence staining for FTase and NLRP3 revealed that FTase expression was elevated in ALF mice along with increased NLRP3 expression (Figure 7A). ELISA assay revealed that PD083176 (d2,d3,d5) treatment reduced the expression levels of TNF- α , IL-1 β and IL-6 in the serum of ALF mice (Figure 7B–D). mRNA levels of TNF- α , IL-1 β and IL-6 were also reduced by RT-PCR (Figure 7E–G). Subsequently, we measured the proteins expression levels of NF- κ B, Caspase-1, NLRP3, IL-1 β , ASC, and GSDMD, which are proteins involved in the development of ALF as the executors of focal death. WB revealed that PD083176(d2,d3,d5) treatment reduced the activity levels of NF- κ B, Caspase-1, NLRP3, IL-1 β , and ASC (Figure 8A–G).

Finally, we investigated necrotic PANoptosis. In ALF mouse liver tissues, RIPK1, RIPK3, and MLKL as well as the increase was inhibited by PD083176(d2,d3,d5) treatment (Figure 8H–K). The above results suggest that the FTase inhibitor PD083176(d2,d3,d5) inhibits PANoptosis in ALF mice. As shown as Figure 9.

Discussion

PD083176 is an early peptide inhibitor designed based on FTase, which is difficult to reach effective concentration in vivo due to poor permeability.²⁰ We constructed a binding model of FTase and PD083176 for the poor tissue permeability of PD083176. Based on the above model, we optimized the structure of PD083176 and designed suitable dosage forms to improve the aqueous solubility and membrane permeability of PD083176 to obtain potentially highly active FTase peptide inhibitors. We preliminarily predicted the binding free energies (affinities) of the 12 designed derivatives for human FTase, and found that the affinities of PD083176(d2, d3, d5) were significantly higher than those of the other sequences. Through a series of animal experiments, we verified that PD083176(d2, d3, d5) has a significant therapeutic effect on ALF in mice.

We went from two models of ALF to demonstrate that the FTase inhibitor PD083176(d2,d3,d5) could prevent ALF in mice. In the LPS/D-GaIN and TAA-induced ALF models, we found that the expression of farnesylated proteins were significantly elevated. Treatment with PD083176(d2,d3,d5) markedly attenuated hepatic proteins farnesylated proteins expression. LPS/D-GaIN or TAA-induced ALF mice mainly exhibit increased mortality, elevated degree of hepatic impairment, elevated histopathological scores of liver pathology, massive apoptosis of hepatocytes and severe inflammatory response. PD083176(d2,d3,d5) treatment significantly ameliorated the progression of ALF and improved survival. Taken together, these observations suggest that the FTase inhibitor PD083176(d2,d3,d5) has an important protective effect against LPS/D-GaIN and TAA-induced ALF in mice.

In the LPS/D-GaIN or TAA-induced acute ALF model, we observed that the areas stained by farnesylated proteins were predominantly hepatocytes. PD083176(d2,d3,d5) inhibited the increase of farnesylated proteins in hepatocytes in ALF mice. Although the current study design does not allow us to determine that farnesylated proteins are responsible for hepatocyte injury after LPS/D-GaIN or TAA attacks. Our results suggest a strong association between excessive farnesylated protein and LPS/D-GaIN or TAA-induced hepatocyte death in D-GaIN/LPS-induced ALF. These findings

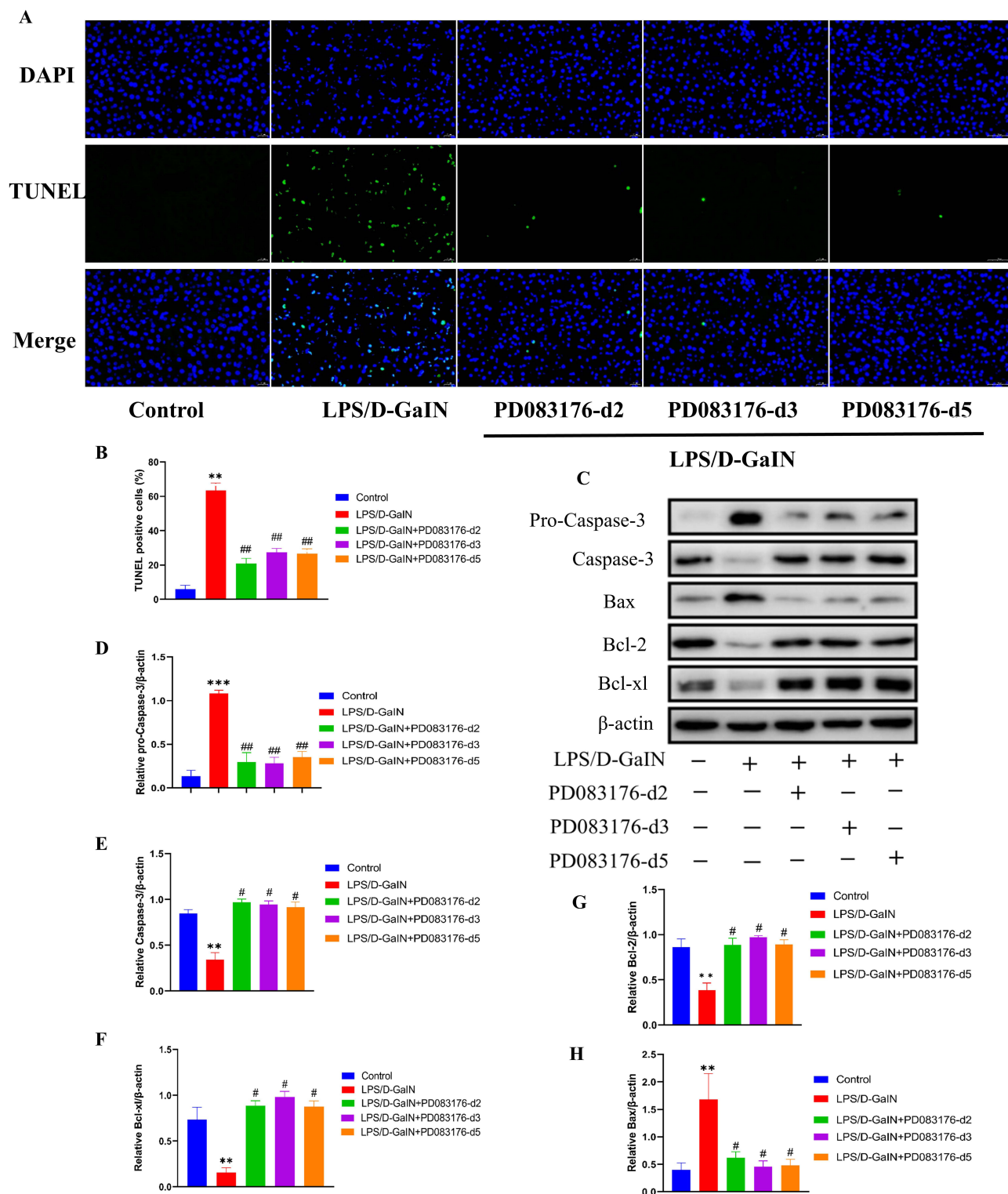


Figure 6 Effect of PD083176(d2,d3,d5) on apoptosis of hepatocytes in each group. **(A)** Apoptotic cells of liver samples were measured by TUNEL staining; **(B)** quantification of apoptosis; **(C)** Protein immunoblotting analysis of Pro-Caspase-3, Caspase-3, Bcl-xl, Bcl-2 and Bax protein expression; Quantitative blotting of Pro-Caspase-3 **(D)**, Caspase-3 **(E)**, Bcl-xl **(F)**, Bcl-2 **(G)** and Bax **(H)**. Compared with the control group, ** $p < 0.01$, *** $p < 0.001$. Compared with the LPS/D-GalN group, # $p < 0.05$, ## $p < 0.001$. $n = 6$ for each group data are expressed as mean \pm SEM.

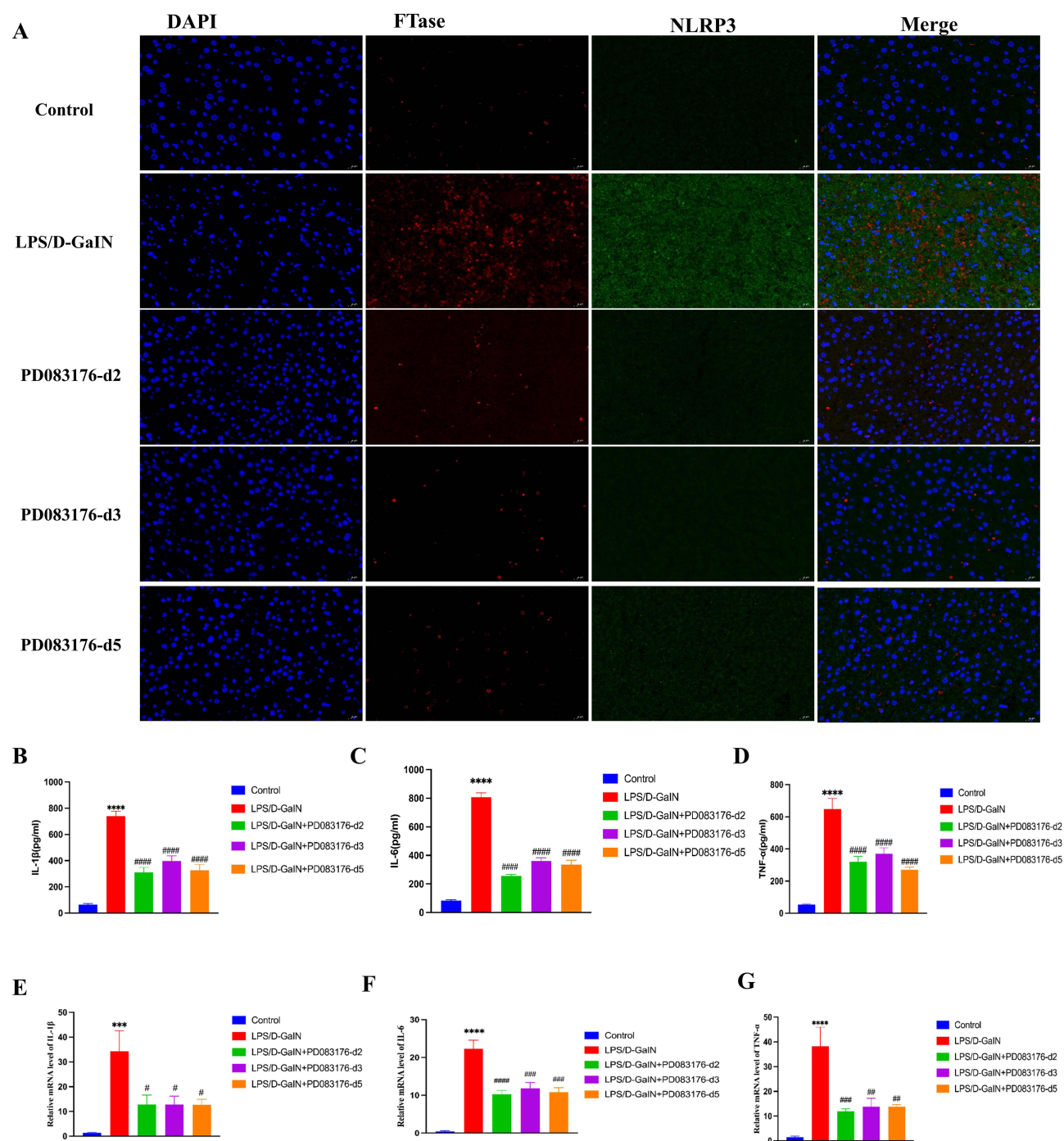


Figure 7 PD083176(d2,d3,d5) attenuates the inflammatory response in LPS/D-GalN-induced acute liver failure. **(A)** Representative images of immunofluorescence double-labeled with NLRP3 (green) and FTase (red) in different groups of ALF mice; ELISA was performed to detect the levels of IL-1 β **(B)**, IL-6 **(C)**, and TNF- α **(D)** in the serum of mice in each group; RT-PCR was performed to detect the expression levels of IL-1 β **(E)**, IL-6 **(F)**, and TNF- α **(G)** in the liver tissues of mice in each group. Compared with the control group, *** p <0.001, **** p <0.0001. Compared with the /LPS/D-GalN group, # p <0.05, ### p <0.01, **** p <0.001, ***** p <0.0001. n = 6 for each group data are expressed as mean \pm SEM.

suggest that farnesylated protein may have a physiological role and that complete inhibition of farnesylated protein may have a negative impact on cell function and viability. In one study, tipifarnib failed to decrease LPS-induced TNF- α secretion from macrophages. Instead, tipifarnib increased the viability of primary hepatocytes incubated with GalN/TNF- α and markedly inhibited the expression of farnesylated proteins in hepatocytes.²⁸

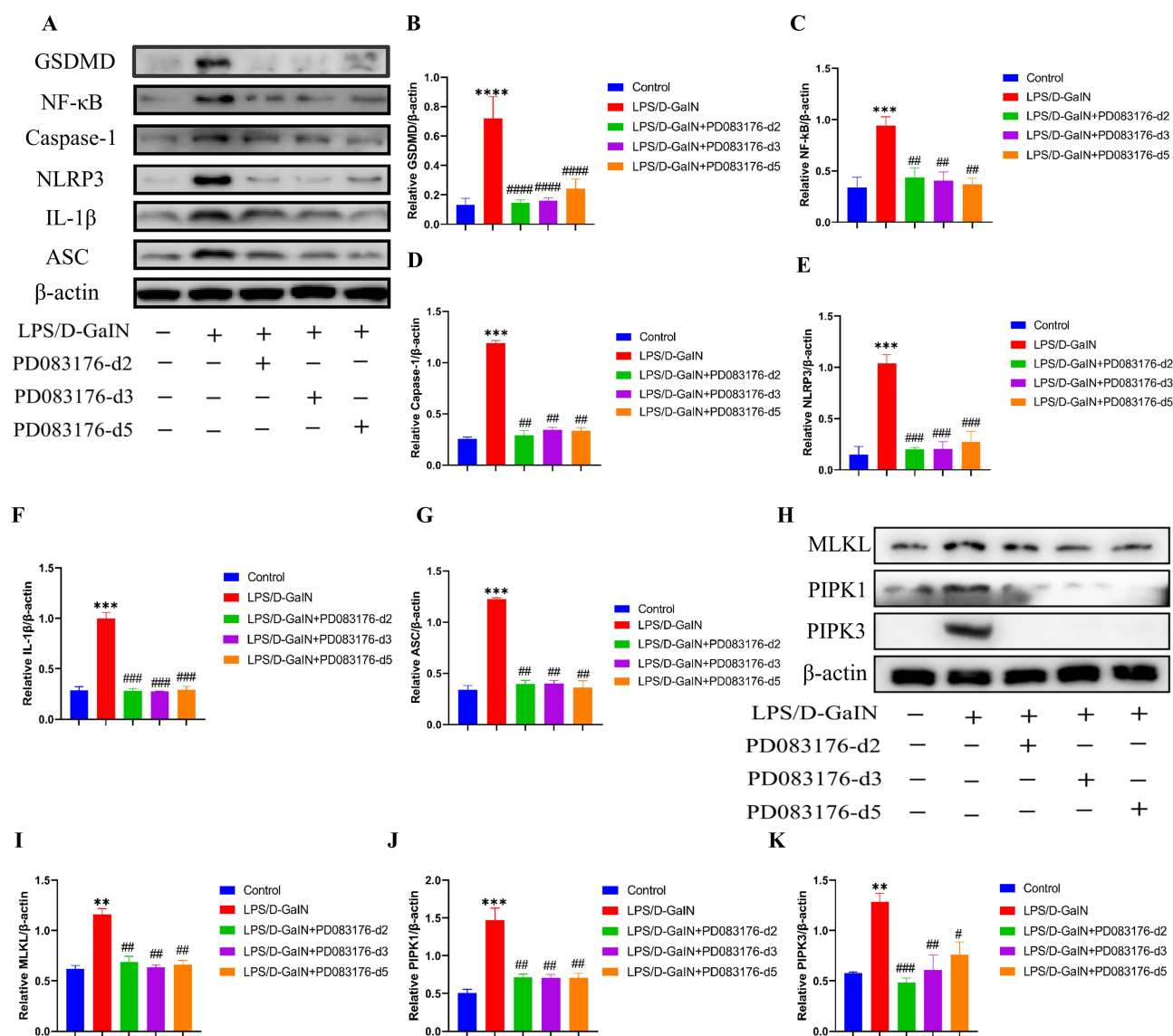


Figure 8 PD083176(d2,d3,d5) blocks the process of necroptosis and pyroptosis in ALF mice. **(A)** Pyroptosis: protein immunoblotting analysis of GSDMD, NF-κB, Caspase-1, NLRP3, IL-1β and ASC protein expression; Quantitative blotting of GSDMD **(B)** NF-κB **(C)**, Caspase-1 **(D)**, NLRP3 **(E)**, IL-1β **(F)** and ASC **(G)**. **(H)** Necroptosis: protein immunoblotting analysis of MLKL, RIPK1, RIPK3 protein expression; Quantitative blotting of MLKL **(I)**, RIPK1 **(J)**, RIPK3 **(K)**. Compared with the control group. * $p < 0.01$, ** $p < 0.001$, *** $p < 0.0001$. Compared with the /LPS/D-GalN group, # $p < 0.05$, ## $p < 0.01$, ### $p < 0.001$, #### $p < 0.0001$. $n = 6$ for each group data are expressed as mean \pm SEM.

In addition to massive hepatocyte death, immune disorders play an important role in the rapid progression of liver failure (LF).²⁹ Alterations in the immune microenvironment in the liver are observed in both ALF and Acute-on-Chronic Liver Failure (ACLF).³⁰ In the case of viral infection, on the one hand, immune cells such as cytotoxic T lymphocytes (CTL) and Natural Killer cells (NKC) are infiltrated in large numbers, and these immune cells secrete perforin and granzyme to induce hepatocyte death; on the other hand, cytokines released by immune cells, such as FasL, TNFα, etc. can be detected in hepatocytes by binding to the Death Ligand receptors on hepatocytes such as Fas, TNFR, etc.^{26,27} Early development of FTase inhibitors was targeted to tumors with RAS mutations.³¹ FTase can inhibit the function of Ras, the T-cell receptor ligand that leads to Ras activation in T-cells, and thus FTase plays a key role in immunomodulation.³² Previous studies have shown that the FTase inhibitor FTI-277 ameliorates the progression of sepsis in a mouse model of sepsis mainly by modulating immune system disorders.³³

The immune system initiates cell death pathways, in response to pathogen and cellular stress. Cell death usually leads to the release of pro-inflammatory cytokines, which can proliferate the immune response.^{34,35} There is a close

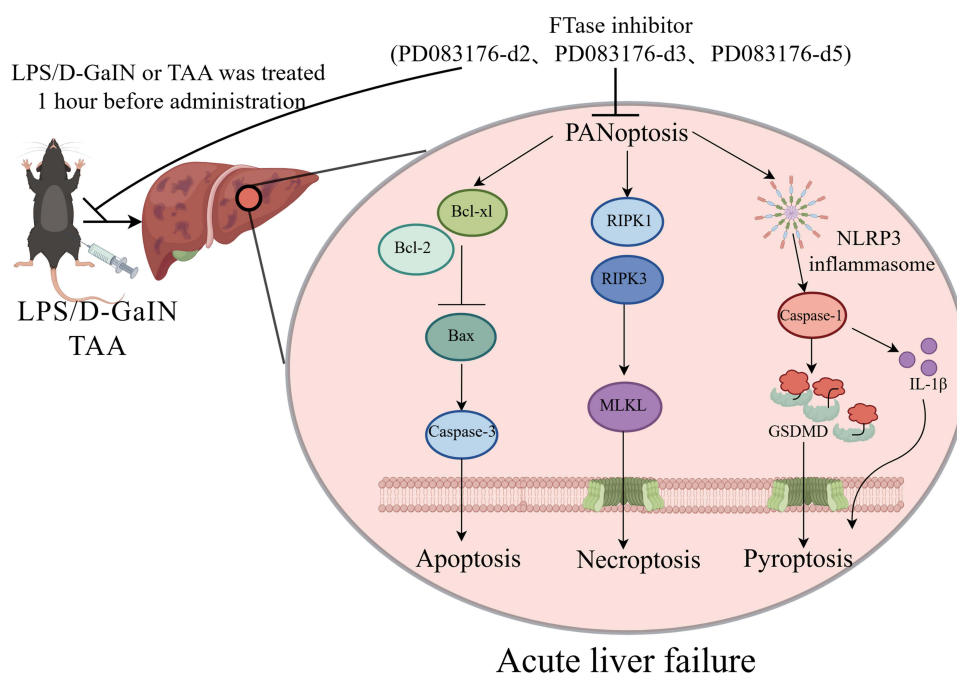


Figure 9 Mechanistic map of the mechanism by which PD083176(d2,d3,d5) may ameliorate ALF progression by regulating PANoptosis. Stimulation by LPS/D-GaIN or TAA resulted in the production of inflammatory factors by a large number of macrophages as well as the occurrence of PANoptosis in a large number of hepatocytes. PD083176 (d2,d3,d5) could attenuate the progression of ALF induced by LPS/D-GaIN or TAA by inhibiting inflammatory response and PANoptosis.

correlation between the inflammatory response and cell death.^{36,37} Our results showed increased expression of PANoptosis-related molecules RIPK1, MLKL, caspase-3, GSDMD, IL-1 β and Bax during ALF, suggesting that elevated levels of PANoptosis occur in LPS/D-GaIN-induced ALF. Figure 9 shown that PD083176(d2,d3,d5) attenuated ALF progression by modulating BAX/Bcl-2/caspase-3, RIPK1/RIPK3/MLKL and NLRP3/GSDMD/IL-1 β pathways in PANoptosis. The caspase family and GSDMD are important molecules in the regulation of pyroptosis, apoptosis, and necroptosis.^{14,38} Caspase-3, Bcl-2, Bcl-x1, and BAX are important apoptosis-regulating molecules.³⁹ Inflammatory vesicles bind to caspase-1 and activated caspase-1 cleaves IL-1 β and IL-18 precursors, promoting the release of IL-1 β and IL-18 and mediating cell death.⁴⁰ RIPK1 is a molecule required for the regulation of PANoptosis and inflammatory responses.⁴¹ RIPK1 recruits NLRP3 and ASC to form a cell-death complex that activates the inflammatory vesicles and GSDMD, leading to pyroptosis and apoptosis.⁴² RIPK1 is also involved in TNF- α -induced PANoptosis driven by FADD/caspase-8 signaling.²³ Therefore, targeting key molecules in PANoptosis may be a novel approach for the treatment of ALF.

The limitations of this study are as follows: We lack the validation of in vivo experiments. We lack long-term efficacy and toxicity data for PD083176(d2,d3,d5). There are many kinds of FTase inhibitors, such as FTI-277,tipifarnib, PD083176 and etc. Therefore, we lack the therapeutic effect of different FTase inhibitors on ALF in the same model. We will do more to improve the above deficiencies in the subsequent experiments to provide stronger evidence for the clinical treatment of FTase inhibitors in ALF.

In summary, high expression of farnesylated proteins in LPS/D-GaIN or TAA-induced ALF mice may play an important role in the development of ALF. We optimized and designed highly active FTase peptide inhibitors. We also verified that the FTase inhibitor PD083176(d2,d3,d5) has multiple effects, including modulation of inflammatory response and blocking of PANoptosis, in LPS/D-GaIN or TAA models of ALF. The study findings might provide a new direction for the treatment of ALF.

Conclusion

In the present study, we demonstrated that we optimized the design to obtain the highly active FTase peptide inhibitor PD083176 (d2,d3,d5). Our animal experiments verified that PD083176 (d2,d3,d5) exerted its effects by inhibiting the

PANoptosis pathway to reduce the production of pro-inflammatory factors and massive apoptosis in hepatocytes. These findings identify FTase as a new potential molecular target for the prevention and/or treatment of ALF. PD083176(d2,d3,d5) may provide new strategies for the treatment of ALF.

Abbreviations

FTase, farnesyltransferase; LPS, lipopolysaccharide; D-GalN, galactosamine; TAA, thioacetamide; ALF, acute liver failure; PCD, programmed cell death; MD, Molecular Dynamics; ACN, Acetonitrile; HPLC, High Performance Liquid Chromatography; DMSO, dimethyl sulfoxide; AST, glutamic oxalacetic transaminase; ALT, glutamic-pyruvic transaminase; TNF- α , tumor necrosis- α ; IL-1 β , interleukin-1 β ; IL-6, interleukin-6; ELISA, enzyme-linked immunosorbent assay; DAPI, Propidium iodide; TUNEL, TdT-mediated dUTP nick end labeling; IHC, Immunohistochemistry; RIPA, radio-immunoprecipitation assay buffer; ACLF, Acute-on-Chronic Liver Failure; CTL, cytotoxic T lymphocytes; NKC, Natural Killer cells; caspase, cysteine aspartate protease.

Data Sharing Statement

FTase Inhibitor PD083176(d2,d3,d5) was produced from Shanghai Gill Biotechnology Ltd (Shanghai, China). The data used to support the findings of this study are included within the article.

Funding

This work was supported by Key Research and Development Project of Zhejiang Province (No. 2023C03046), Basic Public Welfare Research Project of Zhejiang Province (No. LGF19H030013), Taizhou Science and Technology Program (22ywa05).

Disclosure

The authors declare that they have no known competing financial interests or personal relationship.

References

- Shingina A, Mukhtar N, Wakim-Fleming J, et al. Acute liver failure guidelines. *Am J Gastroenterol*. 2023;118(7):1128–1153. doi:10.14309/ajg.0000000000002340
- Vasques F, Cavazza A, Bernal W. Acute liver failure. *Curr Opin Crit Care*. 2022;28(2):198–207. doi:10.1097/MCC.0000000000000923
- Caraceni P, Van Thiel DH. Acute liver failure. *Lancet*. 1995;345(8943):163–169. doi:10.1016/S0140-6736(95)90171-X
- Rajaram P, Subramanian R. Acute liver failure. *Semin Respir Crit Care Med*. 2018;39(5):513–522. doi:10.1055/s-0038-1673372
- Bernal W, McPhail MJ. Acute liver failure. *J Hepatol*. 2021;74(6):1489–1490. doi:10.1016/j.jhep.2021.01.037
- Cheng H, Shi Y, Li X, et al. Human umbilical cord mesenchymal stem cells protect against ferroptosis in acute liver failure through the IGF1-hepcidin-FPN1 axis and inhibiting iron loading. *Acta Biochim Biophys Sin*. 2024;56(2):280–290. doi:10.3724/abbs.2023275
- Montrief T, Koyfman A, Long B. Acute liver failure: a review for emergency physicians. *Am J Emerg Med*. 2019;37(2):329–337. doi:10.1016/j.ajem.2018.10.032
- Dong V, Nanchal R, Karvellas CJ. Pathophysiology of acute liver failure. *Nutr Clin Pract*. 2020;35(1):24–29. doi:10.1002/ncp.10459
- Sowa JP, Gerken G, Canbay A. Acute liver failure - it's just a matter of cell death. *Dig Dis*. 2016;34(4):423–428. doi:10.1159/000444557
- Christgen S, Zheng M, Kesavardhana S, et al. Identification of the PANoptosome: a molecular platform triggering pyroptosis, apoptosis, and necroptosis (PANoptosis). *Front Cell Infect Microbiol*. 2020;10:237. doi:10.3389/fcimb.2020.00237
- Qi Z, Zhu L, Wang K, Wang N. PANoptosis: emerging mechanisms and disease implications. *Life Sci*. 2023;333:122158. doi:10.1016/j.lfs.2023.122158
- Wang Y, Kanneganti TD. From pyroptosis, apoptosis and necroptosis to PANoptosis: a mechanistic compendium of programmed cell death pathways. *Comput Struct Biotechnol J*. 2021;19:4641–4657. doi:10.1016/j.csbj.2021.07.038
- Li W, Zhang W, Zhang D, Shi C, Wang Y. Effect of lipopolysaccharide on TAK1-mediated hepatocyte PANoptosis through Toll-like receptor 4 during acute liver failure. *Int Immunopharmacol*. 2024;129:111612. doi:10.1016/j.intimp.2024.111612
- Shi C, Wang Y, Guo J, Zhang D, Zhang Y, Gong Z. Deacetylated MDH1 and IDH1 aggravates PANoptosis in acute liver failure through endoplasmic reticulum stress signaling. *Cell Death Discov*. 2024;10(1):275. doi:10.1038/s41420-024-02054-8
- Palsuledesai CC, Distefano MD. Protein prenylation: enzymes, therapeutics, and biotechnology applications. *ACS Chem Biol*. 2015;10(1):51–62. doi:10.1021/cb500791f
- Cuddy LK, Alia AO, Salvo MA, et al. Farnesyltransferase inhibitor LNK-754 attenuates axonal dystrophy and reduces amyloid pathology in mice. *Mol Neurodegener*. 2022;17(1):54. doi:10.1186/s13024-022-00561-9
- Widemann BC, Arcenci RJ, Jayaprakash N, et al. Phase I trial and pharmacokinetic study of the farnesyl transferase inhibitor tipifarnib in children and adolescents with refractory leukemias: a report from the Children's Oncology Group. *Pediatr Blood Cancer*. 2011;56(2):226–233. doi:10.1002/pbc.22775

18. Widemann BC, Salzer WL, Arceci RJ, et al. Phase I trial and pharmacokinetic study of the farnesyltransferase inhibitor tipifarnib in children with refractory solid tumors or neurofibromatosis type I and plexiform neurofibromas. *J Clin Oncol.* 2006;24(3):507–516. doi:10.1200/JCO.2005.03.8638
19. Ding J, Chen YX, Chen Y, et al. Overexpression of FNTB and the activation of Ras induce hypertrophy and promote apoptosis and autophagic cell death in cardiomyocytes. *J Cell Mol Med.* 2020;24(16):8998–9011. doi:10.1111/jcmm.15533
20. Leonard DM, Shuler KR, Poulter CJ, et al. Structure-activity relationships of cysteine-lacking pentapeptide derivatives that inhibit ras farnesyltransferase. *J Med Chem.* 1997;40(2):192–200. doi:10.1021/jm960602m
21. Yang W, Wang K, Wu H, Shao H, Chen H, Zhu J. Peptide scaffold-derived peptidomimetic farnesyltransferase inhibitors. *J Chin Chem Soc.* 2021;68(9):1778–1788. doi:10.1002/jccs.202100037
22. Liu GZ, Xu XW, Tao SH, Gao MJ, Hou ZH. HBx facilitates ferroptosis in acute liver failure via EZH2 mediated SLC7A11 suppression. *J Biomed Sci.* 2021;28(1):67. doi:10.1186/s12929-021-00762-2
23. Wang Y, Zhang H, Chen Q, et al. TNF- α /HMGB1 inflammation signalling pathway regulates pyroptosis during liver failure and acute kidney injury. *Cell Prolif.* 2020;53(6):e12829. doi:10.1111/cpr.12829
24. Claeys W, Van Hoecke L, Lefere S, et al. The neuroglial unit in hepatic encephalopathy. *JHEP Reports.* 2021;3(5):100352. doi:10.1016/j.jhepr.2021.100352
25. Kolodziejczyk AA, Federici S, Zmora N, et al. Acute liver failure is regulated by MYC- and microbiome-dependent programs. *Nature Med.* 2020;26(12):1899–1911. doi:10.1038/s41591-020-1102-2
26. Yoon S, Kim TH, Natarajan A, et al. Acute liver injury upregulates microRNA-491-5p in mice, and its overexpression sensitizes Hep G2 cells for tumour necrosis factor- α -induced apoptosis. *Liver Int.* 2010;30(3):376–387. doi:10.1111/j.1478-3231.2009.02181.x
27. Nagaki M, Naiki T, Brenner DA, et al. Tumor necrosis factor α prevents tumor necrosis factor receptor-mediated mouse hepatocyte apoptosis, but not fas-mediated apoptosis: role of nuclear factor- κ B. *Hepatology.* 2000;32(6):1272–1279. doi:10.1053/jhep.2000.20239
28. Shirozu K, Hirai S, Tanaka T, Hisaka S, Kaneki M, Ichinose F. Farnesyltransferase inhibitor, tipifarnib, prevents galactosamine/lipopolysaccharide-induced acute liver failure. *Shock Augusta ga.* 2014;42(6):570–577. doi:10.1097/SHK.0000000000000239
29. Kim SJ, Cho HI, Kim SJ, et al. Protective effect of linarin against D-galactosamine and lipopolysaccharide-induced fulminant hepatic failure. *Eur J Pharmacol.* 2014;738:66–73. doi:10.1016/j.ejphar.2014.05.024
30. Kuhla A, Eipel C, Abshagen K, Siebert N, Menger MD, Vollmar B. Role of the perforin/granzyme cell death pathway in D-Gal/LPS-induced inflammatory liver injury. *Am J Physiol Gastrointest Liver Physiol.* 2009;296(5):G1069–1076. doi:10.1152/ajpgi.90689.2008
31. Kato K, Cox AD, Hisaka MM, Graham SM, Buss JE, Der CJ. Isoprenoid addition to Ras protein is the critical modification for its membrane association and transforming activity. *Proc Natl Acad Sci USA.* 1992;89(14):6403–6407. doi:10.1073/pnas.89.14.6403
32. Pérez de Castro I, Diaz R, Malumbres M, et al. Mice deficient for N-ras: impaired antiviral immune response and T-cell function. *Cancer Res.* 2003;63(7):1615–1622.
33. Yang W, Yamada M, Tamura Y, et al. Farnesyltransferase inhibitor FTI-277 reduces mortality of septic mice along with improved bacterial clearance. *J Pharmacol Exp Ther.* 2011;339(3):832–841. doi:10.1124/jpet.111.183558
34. Rajesh Y, Kanneganti TD. Innate immune cell death in neuroinflammation and alzheimer's disease. *Cells.* 2022;11(12):1885. doi:10.3390/cells11121885
35. Karki R, Kanneganti TD. PANoptosome signaling and therapeutic implications in infection: central role for ZBP1 to activate the inflammasome and PANoptosis. *Curr Opin Immunol.* 2023;83:102348. doi:10.1016/j.coi.2023.102348
36. Zheng M, Kanneganti TD. The regulation of the ZBP1-NLRP3 inflammasome and its implications in pyroptosis, apoptosis, and necroptosis (PANoptosis). *Immunol Rev.* 2020;297(1):26–38. doi:10.1111/imr.12909
37. Oh S, Lee J, Oh J, et al. Integrated NLRP3, AIM2, NLR4, Pyrin inflammasome activation and assembly drive PANoptosis. *Cell mol Immunol.* 2023;20(12):1513–1526. doi:10.1038/s41423-023-01107-9
38. Shi J, Zhao Y, Wang Y, et al. Inflammatory caspases are innate immune receptors for intracellular LPS. *Nature.* 2014;514(7521):187–192. doi:10.1038/nature13683
39. Xie D, Ouyang S. The role and mechanisms of macrophage polarization and hepatocyte pyroptosis in acute liver failure. *Front Immunol.* 2023;14:1279264. doi:10.3389/fimmu.2023.1279264
40. Schwarzer R, Laurien L, Pasparakis M. New insights into the regulation of apoptosis, necroptosis, and pyroptosis by receptor interacting protein kinase 1 and caspase-8. *Curr Opin Cell Biol.* 2020;63:186–193. doi:10.1016/j.ccb.2020.02.004
41. Tao P, Sun J, Wu Z, et al. A dominant autoinflammatory disease caused by non-cleavable variants of RIPK1. *Nature.* 2020;577(7788):109–114. doi:10.1038/s41586-019-1830-y
42. Malireddi RKS, Kesavardhana S, Kanneganti TD. ZBP1 and TAK1: master regulators of NLRP3 inflammasome/pyroptosis, apoptosis, and necroptosis (PAN-optosis). *Front Cell Infect Microbiol.* 2019;9:406. doi:10.3389/fcimb.2019.00406

Drug Design, Development and Therapy

Publish your work in this journal

Drug Design, Development and Therapy is an international, peer-reviewed open-access journal that spans the spectrum of drug design and development through to clinical applications. Clinical outcomes, patient safety, and programs for the development and effective, safe, and sustained use of medicines are a feature of the journal, which has also been accepted for indexing on PubMed Central. The manuscript management system is completely online and includes a very quick and fair peer-review system, which is all easy to use. Visit <http://www.dovepress.com/testimonials.php> to read real quotes from published authors.

Submit your manuscript here: <https://www.dovepress.com/drug-design-development-and-therapy-journal>

Dovepress
Taylor & Francis Group